ADVANCED SUSTAINABLE SYSTEMS
www.advsustainsys.com

Unraveling the Cooperative Activity of Hydrophilicity, Conductivity, and Interfacial Active Sites in Alginate-CNT-Cuo Self-Standing Electrodes with Benchmark-Close Activity for Alkaline Water Splitting

*Mohamed Noufal, Venkata S.N. Chava, Ting Zheng, Srikanth Pilla, Binata Joddar, and Sreeprasad T. Sreenivasan**

Designing electrocatalysts that excel in hydrogen and oxygen electrochemistry is crucial for sustainable hydrogen generation through electrochemical water splitting. This study presents a novel tricomponent catalyst composed of an alginate hydrogel (AL) infused with single-walled carbon nanotubes (CNTs) and copper oxide (CuO) nanoparticles. The catalyst exhibits benchmark-close bifunctional activity toward hydrogen evolution reaction (HER) and oxygen evolution reaction (OER) under alkaline conditions. The aerophobic nature of the AL-gel facilitates superior bubble release from the electrode, while the inclusion of CNTs mitigates charge transfer resistance. Moreover, heterojunctions of CuO and CNTs create unique interfacial active sites, culminating in high electrocatalytic water-splitting activity. The structural rigidity of the composite permits its use as self-standing electrodes (SSE) without using substrates or binders, enabling a direct evaluation of its activity. The composite electrode demonstrates exceptional electrocatalytic HER activity in an alkaline solution, with onset potentials of 93 mV and moderate OER activity with an onset of 155 mV. Moreover, a water electrolysis cell featuring the bifunctional SSE exhibits an open circuit voltage of 1.85 V at 100 mA.cm^{-2}, and only 8% efficiency loss after 100 h marking this a significant stride in developing self-standing nonprecious electrocatalysts with impressive catalytic performance.

1. Introduction

The increasing global energy demand and a growing recognition of the adverse impacts of reliance on fossil fuels as an energy source have spurred extensive research efforts toward developing sustainable and economically viable renewable energy sources.[1] Hydrogen gas (H_2), produced via both photocatalytic and electrocatalytic water splitting, is a promising green fuel that boasts large energy density and carbon emission-free protocols during both production and consumption.[2b,c] However, significant H_2 production from an electrocatalytic water splitting device currently requires the utilization of costly Platinum (Pt) and Ruthenium Oxide (RuO_2)/Iridium Oxide (IrO_2) catalysts—the existing benchmarks to catalyze the two half-cell reactions, the hydrogen evolution reaction (HER), and the oxygen evolution reaction (OER).[2b,2c] The requirement for expensive and scarce catalysts

M. Noufal, S. T. Sreenivasan
Enviromental Sciences and Engineering Program
The University of Texas at El Paso
500 W. University Avenue, El Paso, TX 79968, USA
E-mail: sreenivasan@utep.edu

M. Noufal
Department of Chemical Engineering
Hampton University
Hampton, VA 23668, USA

V. S. Chava, S. T. Sreenivasan
Department of Chemistry and Biochemistry
The University of Texas at El Paso
500 W. University Avenue, El Paso, TX 79968, USA

T. Zheng, S. Pilla
Department of Automotive Engineering
Clemson University
4 Research Drive, Greenville, SC 29607, USA

S. Pilla
Clemson Composites Centre
Clemson University
Greenville, SC 29607, USA

S. Pilla
Department of Materials Science and Engineering
Clemson University
Clemson, SC 29602, USA

S. Pilla
Department of Mechanical Engineering
Clemson Universi Clemson University
Clemson, SC 29602, USA

B. Joddar
Department of Metallurgical, Materials, and Biomedical Engineering
The University of Texas at El Paso
500 W. University Avenue, El Paso, TX 79968, USA

The ORCID identification number(s) for the author(s) of this article can be found under https://doi.org/10.1002/adsu.202300283

DOI: 10.1002/adsu.202300283

to facilitate water splitting makes the derived H_2 expensive and limits its real-world adaptability.[3] Therefore, developing inexpensive, durable, and highly active nonprecious and platinum group metal (PGM)-free electrocatalysts that can match the catalytic performance of current benchmarks for a sustainable H_2 economy can significantly help toward achieving the United Nation's Sustainable Development Goals aiming to "Ensure access to affordable, reliable, sustainable and modern energy for all". Concerted global efforts resulted in the discovery of various classes of catalysts (e.g., nanoparticles, molecular and supramolecular materials, etc.)[4–6] with an abundance of accessible active sites and high surface area, and resultant enhanced catalytic activities.[7] Among these, nanomaterials, characterized by unique band structures, surface areas, and high activities, are among the most promising multifunctional catalyst alternatives.[5,8] Modulating the adsorption energies of the active sites, electronic properties, and the d-band center through chemical modifications can increase the activity of nanocatalysts.[9] Recently, developing nanomaterial-based heterostructures and composites, which possess distinct interfaces and novel active sites, have emerged as a promising pathway to significantly enhance the catalytic activity of nanocatalysts.[10] The altered adsorption energy for intermediates, improved alignment of energy bands, and augmented charge transport provided by the heterostructures at the catalyst-electrolyte interface is responsible for the enhanced catalytic performance.[11]

Another critical factor that can profoundly impact the catalytic performance of an electrocatalyst is its ability to efficiently release the gas bubbles that form at the catalyst surface during HER or OER.[12] This process plays a vital role in maintaining the accessibility of active sites for subsequent reactions. Surprisingly, efforts to enhance bubble release through surface modulation of catalysts have received less attention than those focused on energy optimization of the catalyst. Modifying electrodes to create micro/nanostructured surfaces has demonstrated promising results in accelerating bubble release and enhancing catalytic activity. However, it is essential to acknowledge that the practical application of micro/nanostructured electrodes is limited due to the specific materials to which the fabrication process is applicable and the complexity of the involved fabrication techniques.[13] In contrast, chemical modification offers a highly versatile pathway to enhance surface chemistry and control bubble release, with the advantage of being adaptable to various material systems. In this regard, polymers are particularly advantageous, providing immense flexibility in modifying molecular-level chemistry to achieve desired properties. For instance, by engineering surface functional groups on polymers, it becomes possible to facilitate cross-linking, increase surface area, and fine-tune the hydrophilicity or hydrophobicity of the material.[14]

Among various polymeric systems, hydrogels are particularly noteworthy. Hydrogels are water-insoluble polymeric networks with a remarkable capacity for water absorption, which makes them highly suitable as a platform for catalytic processes involving water. The application of hydrogels in electrocatalytic HER/OER has recently gained traction due to their exceptional bubble release capacity, increased stability, and superior water adsorption-desorption properties.[15] Additionally, hydrogel-based catalysts can function as self-standing electrodes,[16] eliminating the need for traditional substrates such as glassy carbon or carbon cloth. This allows for the direct evaluation of a material's catalytic activity without binders like Nafion, which have been reported to influence electrocatalytic activity.[17] However, the performance of organic entities such as typical hydrogels falls behind that of metal-based catalysts due to their limited electronic conductivity and the lack of d-orbitals, which facilitate the donation or acceptance of electrons during the reaction.[18] Combining the advantages of nanoparticles and polymeric systems, such as hydrogels, through developing polymer-based heterostructures and composites can lead to synergistic effects, resulting in enhanced electrocatalytic performance. This enhancement is achieved by modifying interfacial electronic structures, adsorption energies, and charge transport within the catalysts.[12,18] Furthermore, the abundance of functional groups in polymers allows for precise control of surface chemistry, regulating the adsorption-desorption dynamics of reactants and intermediates, facilitating bubble release, and enabling the simultaneous anchoring of multiple catalytic materials. This capability holds the potential to create multifunctional catalytic systems with diverse activities, offering significant benefits to scientific research and technological applications. Despite these promising prospects, achieving multifunctional activity in hydrogel-based electrocatalysts that can compare to benchmark systems remains a formidable challenge.

In this study, we have developed a self-standing, hydrogel-based composite electrode with remarkable bifunctional HER and OER activity under alkaline pH for the first time. While achieving platinum-like HER activity in acidic environments has become routine, attaining a comparable response in alkaline conditions has proven significantly more challenging, potentially due to the additional water dissociation step required in alkaline HER. Our unique composite, composed of carbon nanotube (CNT) infiltrated Alginate hydrogels and copper oxide (CuO) nanoparticles, has demonstrated benchmark-like HER activity under alkaline conditions. In addition to the ideal energetics in the catalysts, this outstanding performance is partially attributed to the hydrophilic surface structure facilitated by the hydrogel. Alginate (AL), a low-cost, bio-friendly, naturally occurring anionic polymer, is easily gelated by adding divalent cations such as Calcium ions (Ca^{2+}).[19] This characteristic has made alginate-based systems widely useful in biomedical applications.[20] Our recent work demonstrated that integrating sodium dodecyl sulfate (SDS) surfactant-stabilized CNTs into Alginate hydrogel (AL-CNT) leads to a hydrogel matrix with improved conductivity and mechanical stability.[21] Given that mechanical strength, stability, and electrical conductivity are crucial for self-standing electrodes in electrocatalytic applications,[12,22] we utilized our novel AL-CNT hydrogel system as a catalyst platform for electrochemical water splitting. Considering the reported HER and OER efficiencies, CuO nanoparticles (a non-platinum group metal-based oxide) adsorbed over carbon-based materials,[23] we chose to anchor CuO nanoparticles on the AL-CNT hydrogels via an in situ reaction. This led to the creation of a self-standing, precious metal-free, composite catalyst. In our novel Alginate-CNT-Copper oxide tri-component self-standing electrode (Al-CNT-CuO-SSE), each component possesses distinct properties that synergistically work to enhance the overall catalytic activity. The AL-CNT gel addresses the poor conductivity of copper oxide nanoparticles, enhances water adsorption, and improves bubble release.

Meanwhile, the nanomaterials serve as highly active catalytic centers, enabling superior bifunctional OER and HER activities under alkaline conditions. Through Density Functional Theory (DFT) analysis, we have unveiled the underlying principles behind the observed bifunctional activity and identified the active sites. Moreover, we have capitalized on the bifunctional HER-OER activity in alkaline solutions to design a single-cell water-splitting device utilizing AL-CNT-CuO-SSE. Water electrolysis cell featuring the novel bifunctional SSE exhibits an open circuit voltage of 1.85 V at 100 mA.cm^{-2}, and only 8% efficiency loss after 100 h marking this a significant stride in developing self-standing nonprecious electrocatalysts with impressive catalytic performance. Our findings highlight the significant potential of self-standing composite electrodes in enhancing electrocatalytic activity. The advancements made in electrode design and understanding of fundamental principles have the power to open new avenues for improving electrocatalysis. The creation of alternative, PGM-free, self-standing electrodes that can match or even outperform existing benchmark materials is crucial for advancing the United Nations' Sustainable Development Goals (SDGs). Specifically, this innovation could significantly contribute to the SDG of providing universal access to affordable, reliable, and sustainably sourced energy.

2. Results and Discussion

Figure 1a illustrates the preparation of the AL-CNT-CuO-SSE. An AL-CNT hydrogel with a 1 %wt. single-walled CNT (CNT) loading was prepared as previously reported.[24] Copper oxide nanoparticles were then embedded within the AL-CNT hydrogel via an in situ reduction of copper acetate using sodium borohydride for 6 h, forming the AL-CNT-CuO-SSE.[25] The detailed procedure can be found in Section S1 (Supporting Information). The resulting structures were characterized using a variety of microscopic and spectroscopic techniques. X-ray diffraction (XRD) analysis and simulated spectra unveiled the structural details of the sample. A relatively broad feature at 26.05° could be ascribed to the (002) graphitic lattice in CNT, as displayed in Figure 1b. Additional peaks at 2θ = 36.03° (002), 42.3° (202), and 61.59° (213) correspond to the reflections of monoclinic CuO (JCPDS No. 02–1225). This XRD analysis thus confirms the presence of copper oxide in the composite and suggests that the formed nanoparticles could be Copper(II) oxide or cupric oxide (CuO).[26] The simulated structure aligns well with the experimental XRD data, with a minimal difference of 3%, further confirming the formation of the tri-component system as envisioned. The high-resolution Cu 2p X-ray photon spectroscopy (XPS) spectrum (Figure S1a, Supporting Information) presents two distinct peaks at 933.3 and 953.3 eV, corresponding to the Cu $2p_{3/2}$ and Cu $2p_{1/2}$, which once more confirms that the formed particles are of CuO.[27] Thus, XPS confirms the formation of CuO nanoparticles anchored in the Al-CNT gel. Figure S1b (Supporting Information) exhibits the high-resolution C 1s XPS spectrum from the AL-CNT-CuO-SSE composite. The component at 284.69 eV can be assigned to C═C, presumably from CNT. The peak at 286.9 eV corresponds to C—O for COOH groups originating from the alginate polymer.[28] XPS quantification shows that CuO represents 1.87% of the total elemental composition of the prepared AL-CNT-CuO-SSE-10 catalyst (Figure S1c, Supporting Information). The redox characteristics of the AL-CNT-CuO-SSE electrocatalyst were subsequently analyzed using cyclic voltammetry (CV). The CV also confirmed the integration of CuO into the AL-CNT gel. Here, the anchoring of CuO led to a new redox peak at 0.19 V (Figure 1c), ascribed to the redox transformation between CuO and Cu_2O.[29] High-resolution transmission electron microscopy (HRTEM) of the AL-CNT confirmed the presence of CNT inside the Alginate matrix (Figure 1d–j). The CuO morphology was verified as aspherical nanoparticles, as shown in Figure 1f,g. High magnification HRTEM images of AL-CNT-CuO-SSE (Figure 1h) presented lattices with an interplanar spacing of 2.52 Å, which correspond to the (111) lattice plane of CuO.[28,30] Bundles of CNTs were also observed in the image (Figure 1g,i,j). The proximity of CuO nanoparticles to the CNTs also can be seen. This confirms AL-CNT-CuO-SSE formation with CuO anchored on CNT-infiltrated Al hydrogels, as demonstrated in Figure 1g–j. The image clearly shows CuO nanoparticles near the surface of the CNTs, indicating potential heterojunctions between the two nanosystems. Additional HRTEM images depicting the porous structure and CuO nanoparticles in the AL-CNT-CuO-SSE can be found in Figure S2 (Supporting Information). Further, the morphological and elemental characteristics were analyzed using scanning electron microscopy (SEM) and energy-dispersive X-ray spectroscopy (EDS), as depicted in Figure 1k,l, and Figures S3 and S4 (Supporting Information). These images and spectra further confirm the presence of CuO in the AL-CNT-CuO-SSE. A comparison of the SEM and EDS composite images suggests a potentially homogeneous distribution of CuO over the hydrogel in the SSE. To assess the aerophilicity and hydrophilicity, which can influence bubble release in catalysts,[31] we examined the water-contact angle of the electrocatalysts. We utilized a confined bubble design to measure the water contact on Silico dioxide (SiO_2) substrates with and without the hydrogel overlayer (see Figures S5 and S6, Supporting Information). As anticipated, the hydrogel overlayer heightened the hydrophilicity of the underlying substrates, as evidenced by the reduction in water-contact angles from 89.3° (for SiO_2) to 32° (for AL-CNT-CuO-SSE on Silicon), as displayed in Figure S5 (Supporting Information). Among all samples tested, the AL-CNT-CuO-SSE exhibited the smallest water contact angle, indicating it is more hydrophilic than the pristine CNTs and CuO (see Figure S6, Supporting Information). Conversely, this implies that the AL-CNT-CuO-SSE sample will be the least aerophilic.[12] The enhanced hydrophilicity and diminished aerophilicity of the AL-CNT-CuO-SSE can promote faster bubble release, which is crucial for efficiently utilizing active sites during HER and OER.[12]

2.1. Electrochemical Evaluation of AL-CNT-CuO-SSE for Water Splitting

Having confirmed the formation and structure of the composite, we proceeded to investigate its electrocatalytic properties. Due to the significance of electrocatalytic activity in an alkaline medium, we evaluated the electrocatalytic HER and OER activities of AL-CNT-CuO-SSE in 0.1 M potassium hydroxide (KOH) without any additional substrate. Initially, to determine the optimal CuO loading, we examined the charge transfer resistance of the composite with different CuO loadings. Figure S7 (Supporting Information) presents the fitted electrochemical impedance spectrocopy

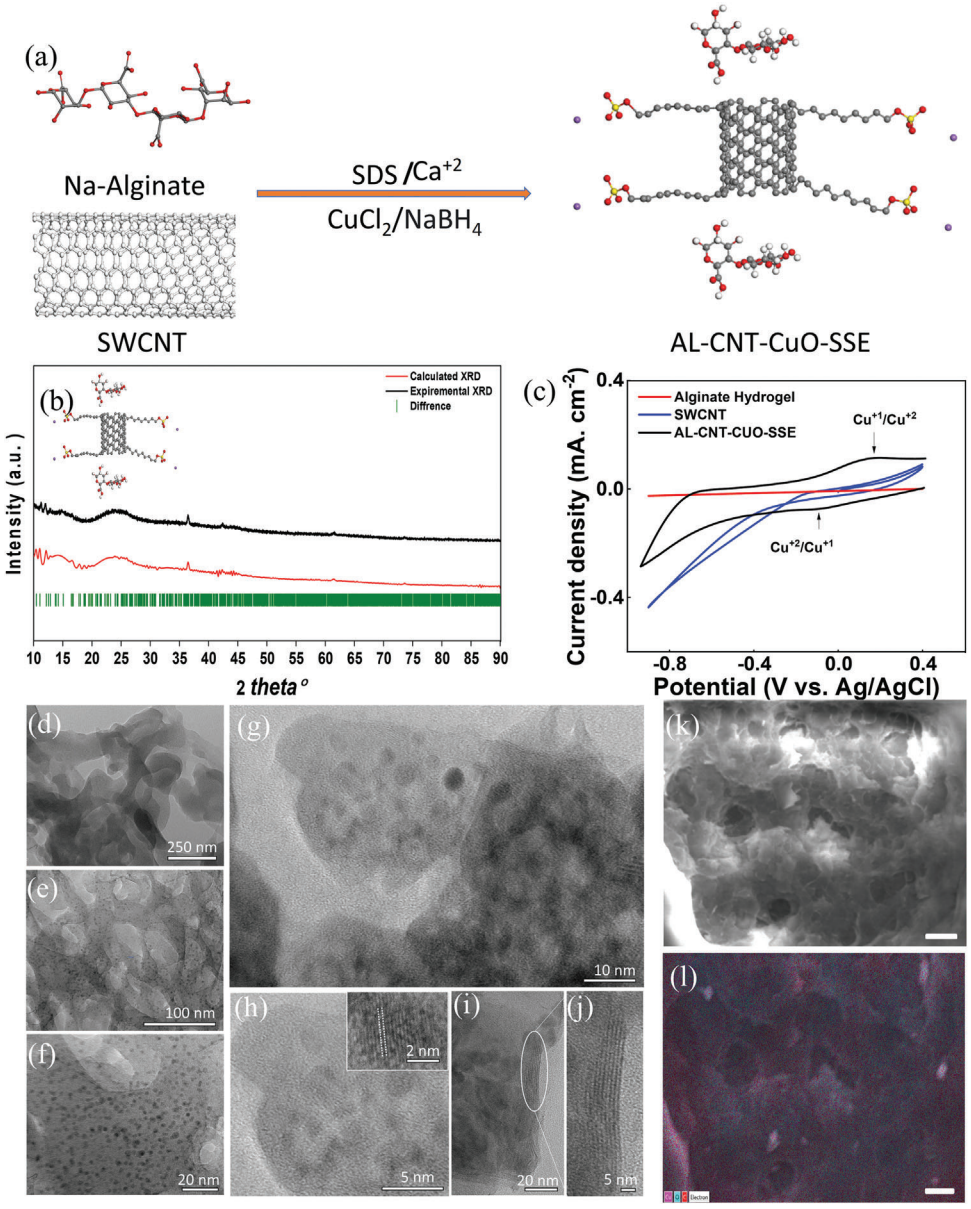

Figure 1. a) Schematic representation of AL-CNT-CuO-SSE synthesis, b) Experimental and simulated X-ray diffraction spectra of the AL-CNT-CuO SSE c) Cyclic voltammetry of the Alginate hydrogel, CNT, and AL-CNT-CuO-SSE, d–j) HRTEM images of the AL -CNT SSE with different magnifications. The lattice fringes from the nanoparticles and SNT bundles can be observed in insets (h–j). k) SEM of AL-CNT-CuO-SS (scale bar is 500 nm) and l) Composite EDS mapping of AL-CNT-CuO SSE from the same region.

(EIS) plots of the AL-CNT-CuO-SSE with varying CuO loadings (1, 5, 10, and 15 ppm of initial Cu precursor loading). Among these, AL-CNT-CuO-SSE with 10 ppm loading demonstrated the smallest semicircle radius, indicating a charge transfer resistance value of 89 Ohm. An additional increase in CuO led to increased charge transfer resistance, possibly due to nanoparticle agglomeration, as evident from the HRTEM images in Figure S8 (Supporting Information). This experiment demonstrates an optimal loading of nanoparticles for the composite that can beneficially influence electrocatalytic performance. This also aligns with the electrochemical surface area measurements obtained from the double-layer capacitance in Figure S9 (Supporting Information). As can be observed CuO with 10 ppm loading shows a higher current density difference and higher double-layer capacitance compared to other loading ratios (Figures S9 and S10, Supporting Information). **Figure 2**a illustrates the HER polarization curves of the as-prepared AL-CNT-CuO-SSE and control electrocatalyst samples, which include Hydrogel, CNT, and CuO. The CNTs and CuO were independently supported on a glassy carbon electrode for the control experiments. The AL-CNT-CuO-SSE exhibited an HER onset potential at 10 mA cm^{-2} of 95 mV, which is remarkably close to the state-of-the-art Platinum/carbon (Pt/C) benchmark electrocatalyst (85 mV).[32] The inferior overpotential values of pure Alginate hydrogel (400 mV), CNT (350 mV),

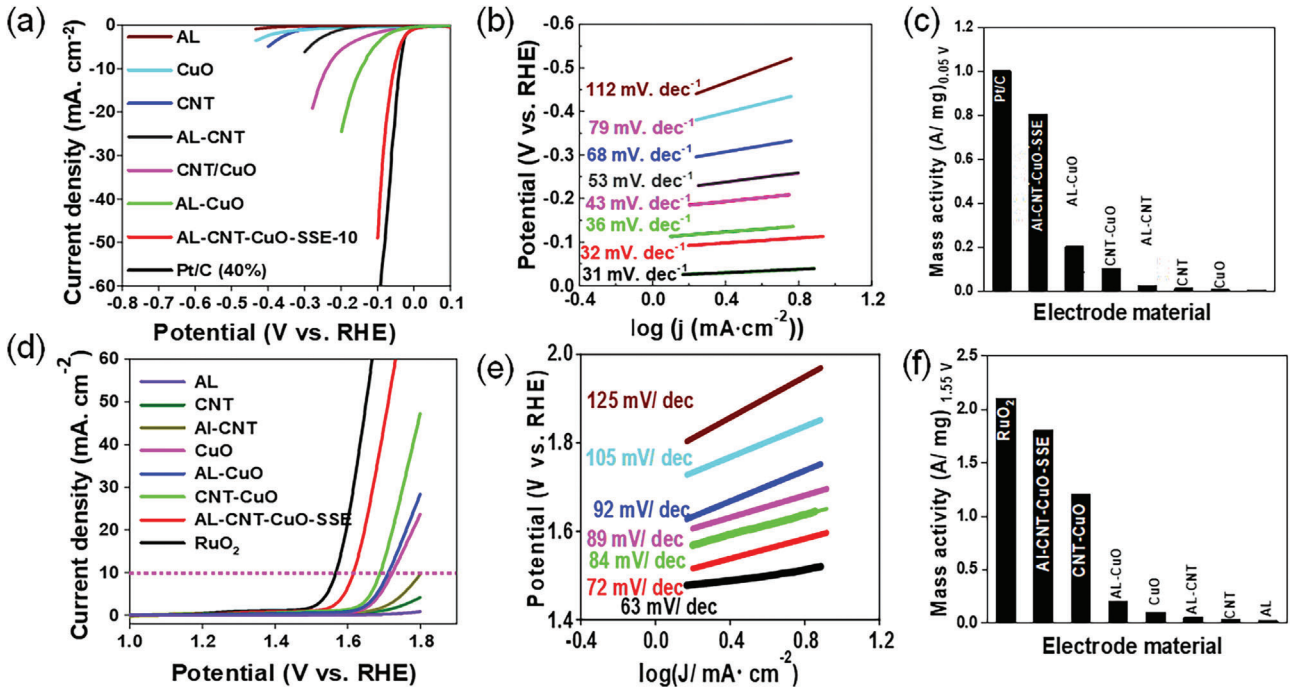

Figure 2. a) Linear sweep voltammetry HER polarization curves, b) the corresponding Tafel slope, and c) HER mass activity chart for the bare Pt/C (40%), CuO, CNT, CNT-CuO, AL-CuO, AL-CNT, and AL-CNT-CuO-SSE. d) OER Polarization plots, e) the corresponding Tafel slope, and f) OER mass activity chart for RuO_2, CuO, CNT, CNT-CuO, and AL-CNT-CuO-SSE.

and CuO (380 mV) indicate potential synergistic effects between the Hydrogel (acting as a hydrophilic material), CNTs, and CuO (serving as conductive materials and potential heterojunction catalytic sites), which contribute to the impressive performance of the AL-CNT-CuO-SSE sample (Figure S11, Supporting Information). We calculated the Tafel slopes for AL-CNT-CuO-SSE to obtain mechanistic insights. As shown in Figure 2b, AL-CNT-CuO-SSE demonstrated a Tafel slope of 32 mV dec^{-1}, suggesting benchmark-like HER activity. The low Tafel slope indicates the facile HER process on AL-CNT-CuO-SSE follows the Tafel-Volmer reaction pathway after the water dissolution step. For further comparison, the HER mass normalized activity was also evaluated (Figure 2c), reaffirming that the HER activity of AL-CNT-CuO-SSE is nearly identical to the Pt/C benchmark.

To evaluate their bifunctional activity, which is advantageous for alkaline water-splitting devices, we assessed the OER activity of the catalyst (from AL-CNT-CuO-10 ppm with the best HER activity). Figure 2d shows the linear sweep voltammetry (LSV) results illustrating the appreciable OER activity of AL-CNT-CuO-SSE with 10 ppm CuO loading with an OER onset potential of 1.55 V (overpotential 320 mV), which is comparable to 1.45 V of RuO_2 (benchmark electrocatalyst for OER) (Figure 2d).[33] Unless otherwise stated, the CuO concentration in the AL-CNT-CuO-SSE composite of 10 ppm was employed for the remaining analyses. The overpotential at 10 mA cm^{-2} (η_{10}) was 470 mV for AL-CNT-CuO-SSE. Moreover, the attained OER performance is comparable to other reported nonprecious OER catalysts (Table S1, Supporting Information). The OER Tafel slope of the AL-CNT-CuO-SSE composite was 72 mV dec^{-1}, <120 mV dec^{-1}, confirming that the Tafel slope decreases remarkably with adding CuO due to abundant OER catalytic sites. This also indicates the fast kinetics in the oxygen evolution reaction, as shown in (Figure 2e).[34] The mass activity of AL-CNT-CuO-SSE exhibits 1.8 A mg^{-1} compared to 2.2 mA mg^{-1} for RuO_2, as displayed in Figure 2f. Lastly, we also examined the electrochemical stability of the AL-CNT-CuO-SSE catalyst by conducting chronopotentiometry measurements at 10 mA cm^{-2}. As demonstrated in the Inset of Figure 2f, the overpotential remains relatively stable for 24 h, thus confirming the excellent stability of the self-standing electrode. We also carried out electrochemical double-layer capacitance (C_{dl}) measurements (Figure S9, Supporting Information), which show the Δj versus scan rate plot of the catalysts at the non-faradaic zone versus the Ag/AgCl reference electrode. Notably, we found that AL-CNT-CuO-SSE yielded the highest values of C_{dl} and electrochemical active surface area (ECSA) among all tested other reference materials, significantly higher than CNT, CuO, and AL-CNT (Figures S9 and S10, Supporting Information). The AL-CNT-CuO-SSE 10 electrode exhibits a high ECSA (14.9 mF cm^{-2}), indicating an abundance of accessible electrochemically active sites. To further illustrate the superiority of the system and to quantify the specific activity toward OER, the turnover frequencies (TOFs) were calculated for all samples. Our calculations demonstrated that the TOF for the Al-CNT-CuO-SSE-10 electrode is 3.2×10^{-3} s^{-1}, which is better than other control catalysts examined in the study. The higher TOF of the AL-CNT-CuO-SSE-10 points to the high specific activity of the active sites present in the catalysts (Figure S10, Supporting Information). Therefore, our EIS, LSV, CV, C_{dl}, and mass activity studies affirm that AL-CNT-CuO-SSE is a promising, highly stable, bifunctional electrocatalyst (HER and OER) with activity near the benchmark system and hence is suitable for water splitting applications.

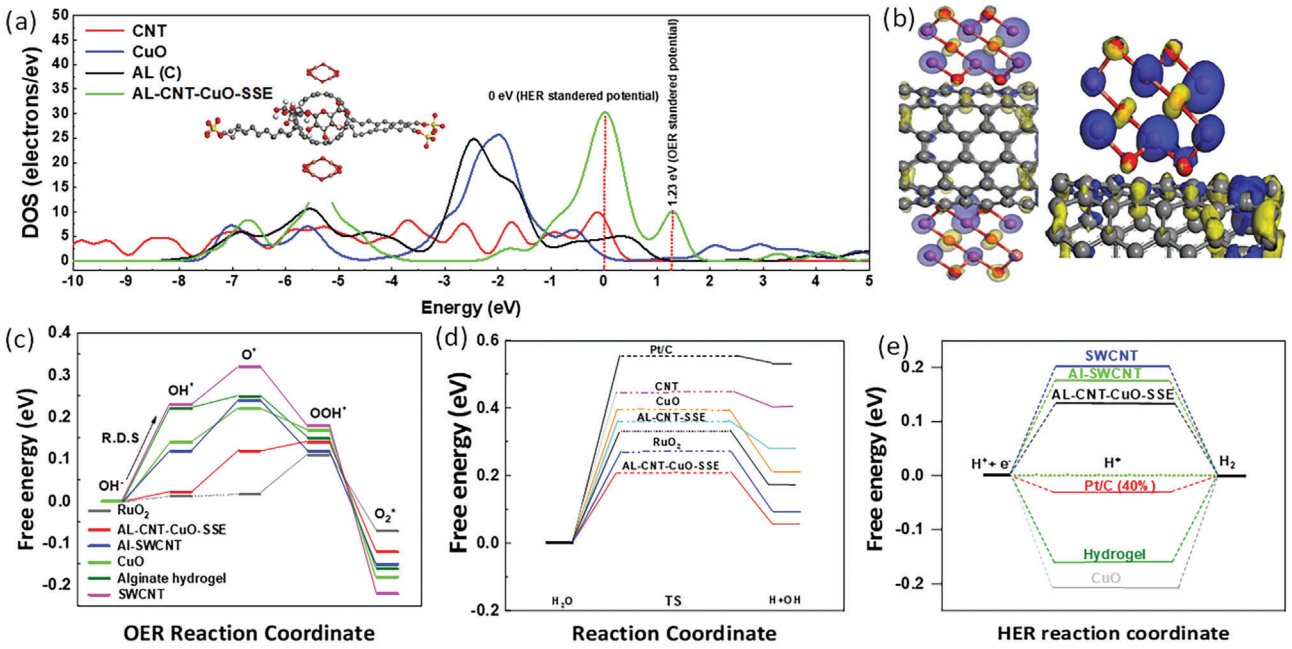

Figure 3. a) TDOS profile of CNT, CuO, Al (C) inside the AL-CNT-CuO-SSE idealized structure and AL-CNT-CuO-SSE, b) Electric field representation of the CuO/CNT interface atoms in the AL-CNT-CuO-SSE idealized structure, c) Comparison of free energy of HER over Alginate hydrogel, CNT, AL-CNT, CuO, AL-CNT-CuO-SSE and AL-CuO electrocatalysts, d) Water dissolution free energy over CNT, AL-CNT, CuO, Pt/C, AL-CNT-CuO-SSE, AL-CuO, and RuO_2 electrocatalysts e) Gibbs Free energy diagram at different steps during the oxygen evolution over Alginate hydrogel, CNT, AL-CNT, CuO, AL-CNT-CuO-SSE, AL-CuO, and RuO_2 electrocatalysts.

2.2. Density Functional Theory (DFT) Studies

To comprehend the observed bifunctional activity of the AL-CNT-CuO-SSE, we applied Density Functional Theory (DFT) to analyze the process. Initially, we idealized the structure of the AL-CNT-CuO-SSE using an Alginate Hydrogel,[35] which comprises irregular blocks of β-D-mannuronic acid (M) and 1–4 linked α-L-guluronic residues (G) that envelop CNT (similar to the AL-CNT experimental sample). CuO is then absorbed over this idealized structure of AL-CNT, and post structure relaxation, it localizes over the CNTs. This supports our HRTEM analysis (Figure 1d–j), where CuO nanoparticles were found close to the CNTs in the SSE. First, we explored the density of states of the CuO, CNT, Alginate hydrogel, and AL-CNT-CuO-SSE. Subsequently, we computed the free energy of intermediates for HER and OER at potentially catalytically active sites. For comparative purposes, free energy for Pt/C (40%) and RuO_2, the benchmark HER and OER electrocatalysts, are also calculated. The density of states (DOS) diagram corresponding to each functional entity inside AL-CNT-CuO-SSE (CuO, CNT, and AL) and the total DOS (TDOS) of the AL-CNT-CuO-SSE is displayed in **Figure 3**a. As can be seen, the DOS of CuO is high near 1.23 V, and the DOS of CNTs is high near the Fermi level (0 V). Also, the TDOS for AL-CNT-CuO-SSE is high near the standard water splitting potential (1.23 V) and Fermi level (0 V). Consequently, the DOS profile supports the experimental observation that the AL-CNT-CuO-SSE is a bifunctional electrocatalyst capable of catalyzing both HER and OER, making it suitable for water-splitting device applications.

The DOS analysis also suggests that CuO is an ideal site for OER, while CNTs exhibit optimal activity for HER. To further verify this, we evaluated the energetics of HER and OER processes at different potential sites on the SSE using DFT. For these DFT calculations, we initially idealized the optimum position of OH adsorption (Table S2 and Figure S12, Supporting Information). Based on our DFT results, we conclude that the copper sites in copper oxide are the active sites for OER, and the carbons of the CNTs that are not connected to the surfactants are the potential active sites for the HER. Electric field distribution with Isovalue (−0.025) shows that positive charges are localized in the Cu sites in CuO and negative charges are localized on the carbons of CNTs inside the AL-CNT-CuO-SSE structure (blue represents positive charge and green represents negative charge) as depicted in Figure 3b. Following this, we calculated the free energy of HER and OER reaction intermediates over these potential active sites. DFT simulations of water dissociation on the RuO_2, AL-CNT-CuO-SSE, CNT, CuO, AL-CNT-CuO, and AL-CNT-CuO-SSE are displayed in Figure 3d. The initial state (H_2O), the transition state (TS), and the final state (H- OH) are indicated in the diagram with the corresponding energy barrier on the surfaces. The AL-CNT-CuO-SSE exhibits a remarkably low activation energy of 0.206 eV required to pass the transition state, which is slightly lower than RuO_2 (0.207 eV), as shown in Figure 3c. Our DFT calculations indicate that the free energy of the HER on AL-CNT-CuO-SSE is −0.07 eV, which is very close to the −0.05 eV value of the Pt/C (40%) benchmark, as depicted in Figure 3d. Here, the OH adsorption over the catalyst constitutes the kinetically limiting reaction step with a TS free energy of 0.25 eV. The free energy value of AL-CNT-CuO-SSE closely resembles that of the RuO_2 benchmark catalyst, as shown in Figure 3e. However, it is worth noting that while CuO exhibits some HER functionality, the activity is

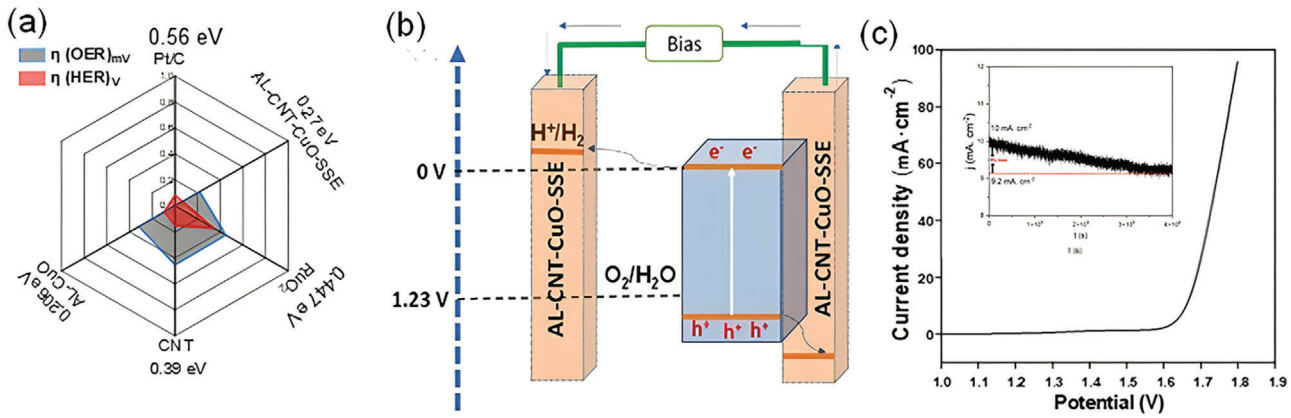

Figure 4. a) Fill chart representation of water dissolution free energy, current density, and OER overpotential for different catalysts explored in the study, b) Schematic representation of water splitting system using AL-CNT-CuO-SSE, and c) Water splitting device polarization curve using AL-CNT-CuO-SSE as both HER and OER electrodes. Inset: Chronoamperometric stability of the water-splitting device for 400 000 s.

inferior to carbon in single-walled carbon nanotubes (CNT) in the present AL-CNT-CuO-SSE configuration. Moreover, the potential electron transfer between CuO and CNTs at the heterojunctions leading to a built-in potential could also contribute to the enhanced HER and OER activity for CNT and CuO catalytic centers in the SSE.

2.3. Water Splitting Device using Self-Standing AL-CNT-CuO-SSE Bifunctional Electrocatalyst

Our analysis reveals that the AL-CNT-CuO-SSE exhibits appreciable bifunctional performance for both HER and OER, comparable to benchmark systems. This excellent activity is illustrated in the line-fill chart of **Figure 4**a, where it is compared to the corresponding benchmarks and the individual components of the SSE. As the AL-CNT-CuO-SSE possesses outstanding electrocatalytic activity under an alkaline medium, a two-electrode water electrolyzer system was set up to further investigate its performance as a self-standing electrode for both the anode and cathode, as shown in Figure 4b. The system was operated in an alkaline KOH electrolyte (0.1 M). Figure 4c demonstrates that the AL-CNT-CuO-SSE requires a cell potential of only 1.85 V to achieve a current density of 10 mA·cm^{-2}, and the electrocatalytic performance of the AL-CNT-CuO-SSE is comparable to recently reported water-splitting devices (see Table S1, Supporting Information). Moreover, the electrochemical stability of the AL-CNT-CuO-SSE catalyst was evaluated by conducting chronoamperometry measurements at a constant voltage of 1.85 V. As shown in the inset of Figure 4c, a minimal loss of ≈8% was observed for the system after 400 000 s, confirming the excellent stability of the AL-CNT-CuO-SSE composite in the water-splitting device.

3. Conclusion

The research unveiled an innovative self-standing, bifunctional electrode rooted in a sustainable polymer matrix, the AL-CNT-CuO-SSE composite, demonstrating exceptional catalytic activity toward HER (onset potential at 10 mA cm^{-2} of 95 mV) and OER (η_{10} = 470 mV) in alkaline conditions. Comprehensive experimental and theoretical studies established superior performance due to a synergistic effect of hydrophilicity, electrical conductivity, and the optimized local electronic configuration in the heterojunctions in the AL-CNT-CuO-SSE composite. A water-splitting device, constructed employing this self-standing AL-CNT-CuO-SSE for both HER and OER, demonstrated a commendable open circuit voltage of 1.85 V and stability (up to 100 h with only ≈8% loss in efficacy), highlighting the supremacy of this material platform and its potential for future applications in electrochemical water-splitting. This research is pivotal in developing cost-effective, non-toxic, and highly active alternative material platforms for electrocatalytic water splitting.

Supporting Information

Supporting Information is available from the Wiley Online Library or from the author.

Acknowledgements

S.T.S. acknowledges the financial support provided through UTEP startup and UT STARs, and the partial support from DOE under grant # DE-EE0010431 and # DE-FE0031908. S.T.S. also acknowledges the partial support through NSF-PREM grant #DMR-1827745. A portion of this research was performed at the Center for Integrated Nanotechnologies, which is an Office of Science User Facility operated for the U.S. Department of Energy (DOE) Office of Science by the Los Alamos National Laboratory (Contract 89233218CNA000001) and the Sandia National Laboratories (Contract DE-NA-0003525). The authors also acknowledge utilizing facilities at the Eyring Materials Center at Arizona State University, partly supported by Nanotechnology Collaborative Infrastructure (NCI)- Southwest by the NSF program NNCI-ECCS-1542160.

Conflict of Interest

The authors declare no conflict of interest.

Data Availability Statement

The data that support the findings of this study are available from the corresponding author upon reasonable request.

Keywords

bifunctional HER and OER activity in Alkaline condition, carbon nanotubes, hydrogels, self-standing electrodes, water-splitting devices

Received: June 29, 2023
Revised: August 30, 2023
Published online: October 19, 2023

[1] a) Y. Fang, Y. Hou, X. Fu, X. Wang, *Chem. Rev.* **2022**, *122*, 4204; b) L. She, G. Zhao, T. Ma, J. Chen, W. Sun, H. Pan, *Adv. Funct. Mater.* **2022**, *32*, 2108465; c) I. Vinogradov, S. Singh, H. Lyle, M. Paolino, A. Mandal, J. Rossmeisl, T. Cuk, *Nat. Mater.* **2022**, *21*, 88.

[2] a) Z. Xie, D. Chen, J. Zhai, Y. Huang, H. Ji, *Appl. Catal., B* **2023**, *334*, 122865; b) T. Xiong, X. Yao, Z. Zhu, R. Xiao, Y.-W. Hu, Y. Huang, S. Zhang, M.-S. (J. T.) Balogun, *Small* **2022**, *18*, 2105331; c) Y. Wang, D. Chen, J. Zhang, M.-S. (Jie Tang) Balogun, P. Wang, Y. Tong, Y. Huang, *Adv. Funct. Mater.* **2022**, *32*, 2112738.

[3] a) S. Ramakrishnan, D. B. Velusamy, S. Sengodan, G. Nagaraju, D. H. Kim, A. R. Kim, D. J. Yoo, *Appl. Catal., B* **2022**, *300*, 120752; b) N. K. Shrestha, S. A. Patil, J. Han, S. Cho, A. I. Inamdar, H. Kim, H. Im, *J. Mater. Chem. A* **2022**, *10*, 8989; c) K. J. Warren, J. T. Tran, A. W. Weimer, *Energy Environ. Sci.* **2022**, *15*, 806.

[4] B. Li, R. Xing, S. V. Mohite, S. S. Latthe, A. Fujishima, S. Liu, Y. Zhou, *J. Power Sources* **2019**, *436*, 226862.

[5] L. Tong, C. Song, Y. Liu, R. Xing, K. Sekar, S. Liu, *Int. J. Hydrogen Energy* **2022**, *47*, 14404.

[6] D. Chanda, R. A. Tufa, Y. Y. Birdja, S. Basu, S. Liu, *Int. J. Hydrogen Energy* **2020**, *45*, 27182.

[7] N. Dubouis, A. Grimaud, *Chem. Sci.* **2019**, *10*, 9165.

[8] N. Kirkaldy, G. Chisholm, J.-J. Chen, L. Cronin, *Chem. Sci.* **2018**, *9*, 1621.

[9] M. Xu, M. Wei, *Adv. Funct. Mater.* **2018**, *28*, 1802943.

[10] a) A. R. Puente Santiago, T. He, O. Eraso, Md. A. Ahsan, A. N. Nair, V. S. N. Chava, T. Zheng, S. Pilla, O. Fernandez-Delgado, A. Du, S. T. Sreenivasan, L. Echegoyen, *J. Am. Chem. Soc.* **2020**, *142*, 17923; b) A. N. Nair, M. F. Sanad, V. S. N. Chava, S. T. Sreenivasan, *Chem. Commun.* **2022**, *58*, 10368.

[11] a) J. Wang, Y. Gao, H. Kong, J. Kim, S. Choi, F. Ciucci, Y. Hao, S. Yang, Z. Shao, J. Lim, *Chem. Soc. Rev.* **2020**, *49*, 9154; b) J. Feng, H. Huang, S. Yan, W. Luo, T. Yu, Z. Li, Z. Zou, *Nano Today* **2020**, *30*, 100830.

[12] D. Jeon, J. Park, C. Shin, H. Kim, J.-W. Jang, D. W. Lee, J. Ryu, *ScienceSci. Adv.* **2020**, *6*, eaaz3944.

[13] a) W.-Z. Chen, M. Zhang, Y. Liu, X.-M. Yao, P.-Y. Liu, Z. Liu, J. He, Y.-Q. Wang, *Appl. Catal., B* **2022**, *312*, 121432; b) L. Lv, Z. Li, Y. Ruan, Y. Chang, X. Ao, J.-G. Li, Z. Yang, C. Wang, *Electrochim. Acta* **2018**, *286*, 172; c) X. Qiao, H. Kang, Y. Li, K. Cui, X. Jia, X. Wu, W. Qin, *Small* **2022**, *18*, 2106378.

[14] a) H. M. El-Husseiny, E. A. Mady, L. Hamabe, A. Abugomaa, K. Shimada, T. Yoshida, T. Tanaka, A. Yokoi, M. Elbadawy, R. Tanaka, *Mater. Today Bio* **2022**, *13*, 100186; b) M. J. Ansari, R. R. Rajendran, S. Mohanto, U. Agarwal, K. Panda, K. Dhotre, R. Manne, A. Deepak, A. Zafar, M. Yasir, S. Pramanik, *Gels* **2022**, *8*, 454; c) F. Damiri, Md. H. Rahman, M. Zehravi, A. A. Awaji, M. Z. Nasrullah, H. A. Gad, M. Z. Bani-Fwaz, R. S. Varma, M. O. Germoush, H. S. Al-Malky, A. A. Sayed, S. Rojekar, M. M. Abdel-Daim, M. Berrada, *Materials* **2022**, *15*, 1666.

[15] a) C. Meng, B. Wang, Z. Gao, Z. Liu, Q. Zhang, J. Zhai, *Sci. Rep.* **2017**, *7*, 41825; b) X. Shan, J. Liu, H. Mu, Y. Xiao, B. Mei, W. Liu, G. Lin, Z. Jiang, L. Wen, L. Jiang, *Angew. Chem., Int. Ed.* **2020**, *59*, 1659.

[16] Y. Guo, J. Bae, Z. Fang, P. Li, F. Zhao, G. Yu, *Chem. Rev.* **2020**, *120*, 7642.

[17] a) F. Yang, L. Xin, A. Uzunoglu, Y. Qiu, L. Stanciu, J. Ilavsky, W. Li, J. Xie, *ACS Appl. Mater. Interfaces* **2017**, *9*, 6530; b) J. C. Jiménez-García, J. A. Olmos-Asar, E. A. Franceschini, M. M. Mariscal, *Phys. Chem. Chem. Phys.* **2021**, *23*, 27543.

[18] S. Chen, J. Duan, M. Jaroniec, S. Z. Qiao, *Angew. Chem., Int. Ed.* **2013**, *52*, 13567.

[19] M. Stephen, A. Nawaz, S. Y. Lee, P. Sonar, W. L. Leong, *Adv. Funct. Mater.* **2023**, *33*, 2208521.

[20] X. Lin, J. Wang, X. Wu, Y. Luo, Y. Wang, Y. Zhao, *Adv. Funct. Mater.* **2023**, *33*, 2211323.

[21] G. Lemercier, E. Mulliez, C. Brouca-Cabarrecq, F. Dahan, J.-P. Tuchagues, *Inorg. Chem.* **2004**, *43*, 2105.

[22] a) Y. Lin, Z. Tian, L. Zhang, J. Ma, Z. Jiang, B. J. Deibert, R. Ge, L. Chen, *Nat. Commun.* **2019**, *10*, 162; b) B. Wang, P. Zhao, J. Feng, D. Chen, Y. Huang, L. Sui, H. Dong, S. Ma, L. Dong, L. Yu, *J. Colloid Interface Sci.* **2021**, *588*, 184.

[23] a) Y. Zhang, Z. Yan, M. Zhang, Y. Tan, S. Jia, A. Liu, *Appl. Surf. Sci.* **2021**, *548*, 149218; b) D. Xu, K. C. Chan, H. Guo, H. Zhong, L. Lu, *J. Mater. Chem. A* **2021**, *9*, 16470; c) X.-Y. Yan, X.-L. Tong, Y.-F. Zhang, X.-D. Han, Y.-Y. Wang, G.-Q. Jin, Y. Qin, X.-Y. Guo, *Chem. Commun.* **2012**, *48*, 1892.

[24] F. Alvarez-Primo, S. Anil Kumar, F. S. Manciu, B. Joddar, *Int. J. Mol. Sci.* **2019**, *20*, 4802.

[25] S. M. Roopan, D. Devi Priya, S. Shanavas, R. Acevedo, N. A. Al-Dhabi, M. V. Arasu, *Mater. Sci. Eng., C* **2019**, *101*, 404.

[26] N. Bouazizi, R. Bargougui, A. Oueslati, R. Benslama, *Adv. Mater. Lett.* **2015**, *6*, 158.

[27] a) Y. Li, S. Chu, H. Shen, Q. Xia, A. W. Robertson, J. Masa, U. Siddiqui, Z. Sun, *ACS Sustainable Chem. Eng.* **2020**, *8*, 4948; b) J. Yuan, J.-J. Zhang, M.-P. Yang, W.-J. Meng, H. Wang, J.-X. Lu, *Catalysts* **2018**, *8*, 171.

[28] A. Jejurikar, X. T. Seow, G. Lawrie, D. Martin, A. Jayakrishnan, L. Grøndahl, *J. Mater. Chem.* **2012**, *22*, 9751.

[29] H. Naatz, S. Lin, R. Li, W. Jiang, Z. Ji, C. H. Chang, J. Köser, J. Thöming, T. Xia, A. E. Nel, L. Mädler, S. Pokhrel, *ACS Nano* **2017**, *11*, 501.

[30] M. He, H. Jiang, B. Liu, P. V. Fedotov, A. I. Chernov, E. D. Obraztsova, F. Cavalca, J. B. Wagner, T. W. Hansen, I. V. Anoshkin, E. A. Obraztsova, A. V. Belkin, E. Sairanen, A. G. Nasibulin, J. Lehtonen, E. I. Kauppinen, *Sci. Rep.* **2013**, *3*, 1460.

[31] G. Liu, W. S. Y. Wong, M. Kraft, J. W. Ager, D. Vollmer, R. Xu, *Chem. Soc. Rev.* **2021**, *50*, 10674.

[32] a) Z. Chen, H. Qing, R. Wang, R. Wu, *Energy Environ. Sci.* **2021**, *14*, 3160; b) J. Yu, Y. Guo, S. She, S. Miao, M. Ni, W. Zhou, M. Liu, Z. Shao, *Adv. Mater.* **2018**, *30*, 1800047; c) H. Tan, B. Tang, Y. Lu, Q. Ji, L. Lv, H. Duan, N. Li, Y. Wang, S. Feng, Z. Li, C. Wang, F. Hu, Z. Sun, W. Yan, *Nat. Commun.* **2022**, *13*, 2024.

[33] R. Jiang, D. T. Tran, J. Li, D. Chu, *Energy Environ. Mater.* **2019**, *2*, 201.

[34] T. Shinagawa, A. T. Garcia-Esparza, K. Takanabe, *Sci. Rep.* **2015**, *5*, 13801.

[35] H.-R. Lee, S. M. Jung, S. Yoon, W. H. Yoon, T. H. Park, S. Kim, H. W. Shin, D. S. Hwang, S. Jung, *Sci. Rep.* **2019**, *9*, 12357.